Geomorphology 259 (2016) 55–69

Contents lists available at ScienceDirect

Geomorphology

journal homepage: www.elsevier.com/locate/geomorph

Tectonic geomorphology of a large normal fault: Akşehir fault, SW Turkey

Savaş Topal [a], Edward Keller [b,*], Aaron Bufe [b], Ali Koçyiğit [c]

[a] Pamukkale University, Engineering Faculty, Department of Geological Engineering, Kınıklı Campus, 20017 Denizli, Turkey
[b] Department of Earth Science, University of California, Santa Barbara, CA 93106, USA
[c] Middle East Technical University, Department of Geological Engineering, Tectonic Research Unit, TR-06531, Ankara, Turkey

ARTICLE INFO

Article history:
Received 7 August 2015
Received in revised form 21 January 2016
Accepted 22 January 2016
Available online 23 January 2016

Keywords:
Tectonic geomorphology
Active tectonics
Geomorphic indices
Mountain front facets

ABSTRACT

In order to better understand the activity of the Akşehir normal fault in SW Turkey and the associated seismic hazard, we investigated the tectonic geomorphology of a 60-km stretch of the 100-km-long Akşehir fault block. The fault can be separated into seven geomorphic segments (1 to 7 from NW to SE) along the mountain front. Segment length varies from about 9 to 14 km, and relief of the horst block varies from about 0.6 km in the SE to 1.0 km in the NW. Analysis of the tectonic geomorphology of 32 drainage basins and mountain front facets using a combination of geomorphic indices reveals a general pattern of high slip rates in the northern and central segments and low slip rates in the southern, probably older, segments. We show that mountain front sinuosity varies from about 1.1 to 1.4 on segments S1-S6 to 2.4 on segment S7, suggesting that the six northern segments are more active than the southernmost segment. Similarly, χ analysis and slope-area analysis of streams reveal a pattern of steepest channels draining the central and northern segments of the horst. The ratio of valley floor width to valley height varies from 0.2 to 0.6, which are typical values for tectonically active mountain fronts; and alluvial fans along segments S1, S2, and S4 are back-tilted. Finally, we show that (1) shapes of the ~100–900m high mountain front facets are mostly triangular (~80%) and partly trapezoidal (~20%); (2) facet slopes range from 6 to 22°; (3) facets at the NW and SE segment ends are larger than the intervening facets; and (4) steepest facets occur along the central segments. Uplift rates estimated from the slope of mountain front facets range from about 0.06 m/ky on the southernmost fault segment (S7) to 0.23 m/ky on the more central S5 and 0.16 m/ky on the northern segment (S1). The estimated pattern of uplift is consistent with the pattern of geomorphic indices. The vertical relief of the facets suggests that uplift of the mountain front initiated in the late Miocene-early Pliocene and continues to the present, with the earliest surface-rupturing faults on the southernmost fault segment (S7).

Large normal faults with a similar slip rate of 0.2–0.3 m/ky typically have strong earthquakes every few thousand years. Therefore, the many moderate to strong earthquakes on the Akşehir fault in the past few hundred years may be misleading. A paleoseismic evaluation could answer questions concerning the area's earthquake hazard. The tectonic geomorphology suggests that the Akşehir fault is active, and larger earthquakes than those of the historic period are a potential threat.

1. Introduction

1.1. Research objectives

The overall objective of this work is to better understand the tectonic geomorphology of the Akşehir normal fault in SW Turkey. Specific objectives are to (i) evaluate mountain front tectonic geomorphology by using a variety of indices to reveal patterns of recent tectonic activity, (ii) estimate vertical rates of uplift for specific mountain front geomorphic segments, and (iii) discuss these findings in the light of seismic hazard of the Akşehir region.

1.2. Previous work

The study of normal faults has a long, rich history of investigation. More recently, the application of geomorphic principles is leading to a better understanding of the geomorphic history and active tectonics of normal faults. For a summary of tectonic geomorphology of normal faults, see Keller and Pinter (2002) and Burbank and Anderson (2012).

Mountain fronts generated by normal faulting have fascinated geomorphologists for over 100 years. These include Davis (1903), Louderback (1904), Blackwelder (1928), and Gilbert (1928). More recent investigations include Wallace (1978) and Bull (2007), Menges (1990), DePolo and Anderson (2000), and Burbank and Anderson (2012). Much of the earlier work was focused on a better understanding of the Basin and Range Physiographic Province of the southwestern United States. The region is characterized by many horst and graben

* Corresponding author.
E-mail address: keller@geol.ucsb.edu (E. Keller).

http://dx.doi.org/10.1016/j.geomorph.2016.01.014
0169-555X/

structures that were described by the famous geologist Clarence Dutton as an army of caterpillars marching northward out of Mexico (in Keyes, 1909; this may not be the primary reference, which is unknown).

Quantitative research on the geomorphology of mountain fronts began in the 1970s with seminal work by Bill Bull (Bull and McFadden, 1977). This work developed several geomorphic indices, such as mountain front sinuosity and valley width-to-height ratios that have shown through numerous studies to be valuable in understanding relative tectonic activity of mountain fronts generated by normal faults (Keller and Pinter, 2002), despite problems in some settings. In addition to those classic geomorphic indices of mountain front geomorphology, stream profile analysis has emerged as a significant tool in understanding active tectonics in erosional landscapes and is based on the prediction that stream profiles respond to external forcings of rock uplift/subsidence, sediment flux, and water discharge by changing their gradient (c.f. Kirby and Whipple, 2012, for a review). While such geomorphic indices reveal broad patterns of deformation, assigning a slip rate to such patterns requires additional information.

Estimation of vertical slip rates of normal faults has traditionally been through excavation of trenches along faults and by dating offset units (Keller and Pinter, 2002; Burbank and Anderson, 2012). While this has been extremely valuable in evaluating the earthquake hazard during the Holocene and late Pleistocene, it has not been particularly useful in determining long- term vertical slip rates that produce faceted mountain fronts with several hundred meters and more of vertical relief. Recent work suggests that the shape of mountain front facets can be used to estimate vertical slip rates. Such triangular facet or faceted spurs are one of the most striking features of mountain fronts produced by active normal faulting and were discussed eloquently by Wallace (1978). Wallace noted that the classical use of the term triangular facet is somewhat misleading, in that many facets are trapezoids or more complex features that increase in complexity through time because of erosion of the mountain front (Wallace, 1978). The important contribution of Wallace (1978) was the idea that tectonic landforms such as faceted spurs evolved through time as a direct response to uplift and erosion. Facets are considered to be eroded fault scarps and, as such, will change through time from mountain front scarps to eroded fault scarps of lesser inclination. Given sufficient time, a piedmont of relatively low relief may result from a low rate of vertical uplift relative to erosion. On the contrary, with more rapid ongoing uplift, the faceted mountain front may be preserved for hundreds of thousands of years to perhaps several million years. Based on such considerations, DePolo and Anderson (2000) compiled known vertical slip rates and basal facet heights for normal faults in a subregion of the Great Basin and developed a simple statistical model that allowed vertical slip rates to be estimated on several hundred normal faults in Nevada. The model of DePolo and Anderson (2000) was applicable to normal faults with a vertical slip rate exceeding 0.1 m/ky and applied to a range of slip rates from ~0.1 to 2.0 m/ky.

Tsimi and Ganas (2015) analyzed 232 mountain front facets along 10 normal faults with known slip rates to develop a relationship between facet slope and vertical slip rate. Tsimi and Ganas also evaluated the relationship between known vertical slip rate and facet height. They found that the relationship between facet slope and vertical slip rate was statistically stronger than for facet height. The dependence of facet slope on vertical slip rate is not particularly surprising, as we view mountain front facets as eroded fault scarps that directly reflect active faulting. Therefore, a low slope of a facet may reflect a low slope of the fault or fault scarp degradation, both of which might lead to a relationship between scarp slope and vertical slip rate. What is clear from the previous work on mountain front facet geomorphology, whether it be facet height or slope, is that both parameters are evidently in part related to the vertical slip rate of the range-bounding fault. Differentiating which of the two parameters provide the best estimate of the vertical slip rate is difficult at this time, but intuitively, the slope of a mountain front facet would seem to be directly related to the vertical slip rate (as well as the strength of the rock, the climate, etc.), whereas the height of the facet might be related to the time since faulting initiated in addition to the slip rate.

In this contribution, we analyze the pattern of Quaternary tectonic activity along the Akşehir normal fault in SW Turkey, using a combination of geomorphic indices and stream profile analysis. We then explore facet shapes and use facet slopes to estimate slip rates on the normal fault. Finally, we discuss these findings in the context of the seismic hazard in the Akşehir region.

1.3. Study area

The focus of this study is a 60-km stretch along the Sultandağı–Akşehir Horst from Çay in the northwest to Doğanhisar in the southeast (Fig. 1), encompassing over half the length of the 100-km long Akşehir fault. Relief of the horst varies from about 1000 m in the northwest to 600 m in the southeast. The mountain front from Çay to Doğanhisar is relatively straight, with deeply incised (wineglass-shaped) valleys draining into the Akşehir graben. Four prominent alluvial fans are located between Çay and Akşehir (Fig. 1B).

The climate of the piedmont area at the foot of the horst block at Akşehir is Mediterranean, characterized by warm, dry summers and cool, wet winters. Average annual rainfall is about 600 mm at Akşehir and, presumably, considerably higher at the crest of the horst block with elevation exceeding 1 km.

1.4. Regional and local geological framework

The regional tectonic framework is shown in Fig. 1A, and the more local tectonic framework is shown in Fig. 1B. On a regional scale, tectonic processes in SW Turkey are controlled by the convergence of the Arabian and Eurasian plates, as well as the subduction of the African plate beneath the Eurasian Plate (Fig. 1A). Caught between the converging plates, the Anatolian Platelet moves westward along major strike-slip systems and shows a complex pattern of internal strike slip and extensional faulting (Fig. 1A). To the south, the African plate subducts along the Strabo-Pliny and the Cypress trenches, which form a sharp right angle. That right angle appears to control the geometries of the Inner and Outer Isparta Angles to the north. Of particular importance to the present study is the Outer Isparta Angle. The apex of the Outer Isparta Angle is thought to be a very important tectonic structure with significant geomorphic expression that is linked to the western movement (escape) of the Anatolian Platelet. The general consensus is that the Outer Isparta Angle is formed by two normal fault zones; the Akşehir fault zone (of this study) and the Fethiye–Burdur fault zone that meet at approximately right angles producing radial extension and domal uplift (Koçyiğit and Özacar, 2003). For a review of the geology of the Isparta Angle, see Piper et al. (2002); Koçyiğit and Özacar (2003); Ten Veen (2004), and Koçyiğit et al. (2013). Along the northeast edge of the Outer Isparta Angle lies the Akşehir graben, bounded to the south by the Akşehir fault and to the north by the Karagöztepe fault zone (Fig. 1B).

The Akşehir fault is a normal fault with a small component of strike slip. Based on modeling the 2000 Sultandağı and 2002 Çay earthquakes, the Akşehir fault has an average dip of about 60° to the NE (Koçyiğit and Özacar, 2003). Thus, the expected block rotation of the large normal fault (e.g., Jackson and White, 1989) would explain the observed back tilting of the Akşehir horst block to the southwest (Emre et al., 2003). In the northern part of the Akşehir horst, the tilt becomes progressively more south- and southeastward because of the influence of east–west and northeast-southwest striking normal faults (Emre et al., 2003). Total maximum vertical slip rate of 0.3 m/ky since the late Pliocene was estimated for the main Akşehir fault by using ages from mammalian fossils in alluvial fan deposits (Koçyiğit and Özacar, 2003).

The dominant rock types in the Sultandağı–Akşehir Horst block are Paleozoic sedimentary rock (siltstone, claystone, and sandstone) and, closer to the mountain front, resistant Paleozoic and Mesozoic metamorphic rocks (quartzite, schist, and marble) (Fig. 2). The Akşehir graben is dominated by Quaternary sandstones and mudstones and four young alluvial fans emerging from the horst block from Akşehir to Çay. We propose seven geomorphic segments of the Akşehir fault, based on the geomorphic expression where stepovers or bends in the fault occur (Fig. 2).

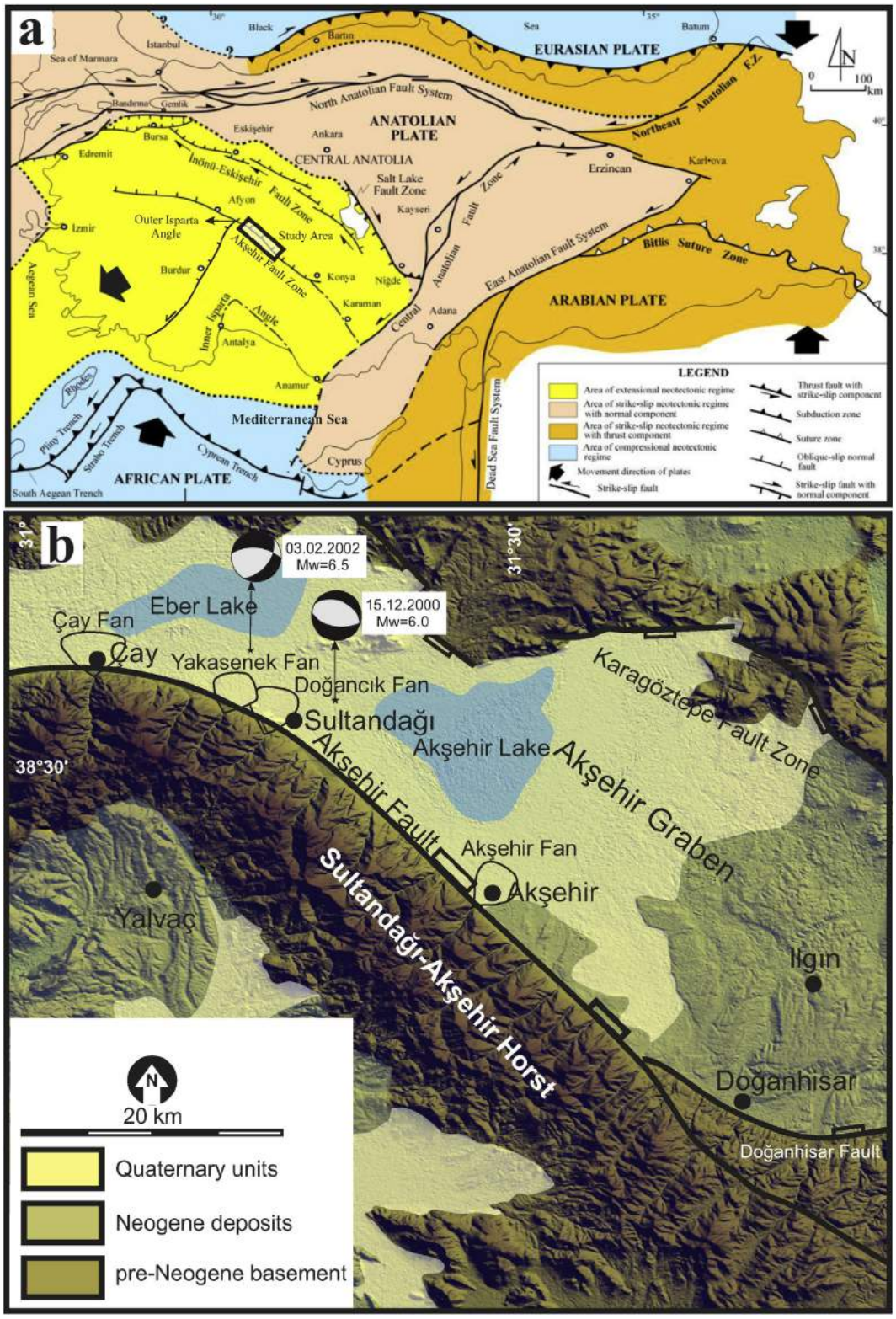

Fig. 1. A) Regional tectonic framework, showing the study area near the Outer Isparta Angle; B) local tectonic framework at the Akşehir fault, with epicenters of 2000 and 2003 earthquakes; and C) Google Earth image, showing the straight mountain front near Akşehir. A and B are modified from Koçyiğit and Özacar, 2003.

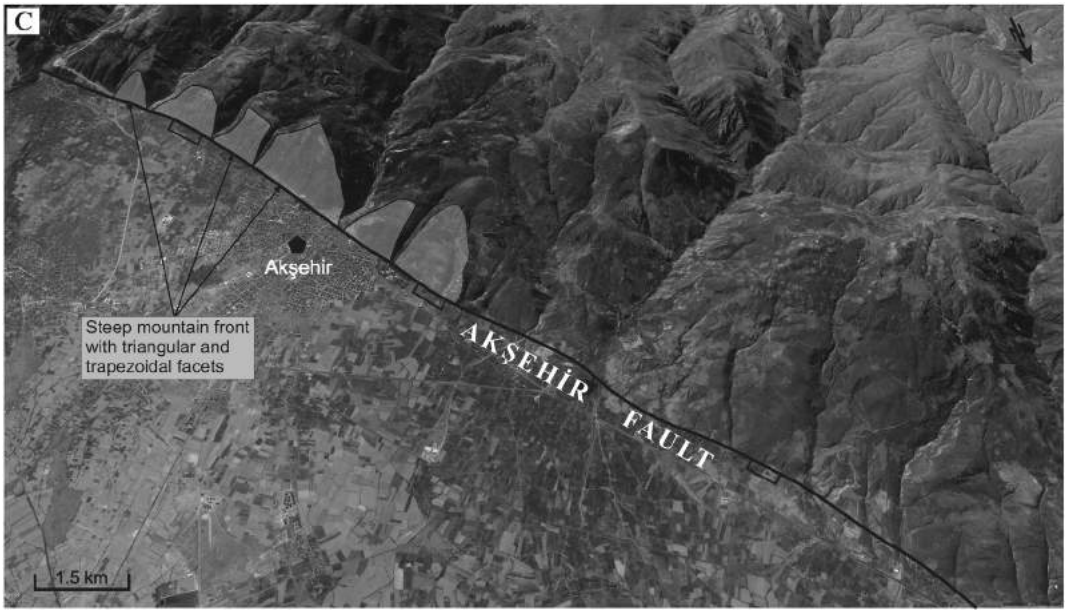

Fig. 1 (*continued*).

1.5. Seismicity

Seven seismic events with Modified Mercalli Intensities from VI to X occurred at the towns of Afyon, Şuhut, and Ilgın from A.D. 94 to B.C. 1899 (Ergin et al., 1967). A catalog of 45 earthquakes in the Akşehir graben system from 1776 to 1964 is provided by Özer (2006). Unfortunately, reliable data on the exact location of the epicenter; the depth of the hypocenter; the time, magnitude, and source of the earthquake; and the structural damage and number of casualties caused by these seismic events do not exist. The Şuhut graben, which is located 7 km south of the Akşehir fault zone, was the epicenter of the 1862 earthquake of Mercalli Intensity X (Koçyiğit and Deveci, 2007). During this earthquake, the town of Şuhut was heavily damaged by numerous foreshocks and the main shock. Eight hundred people were killed, and severe damage was reported from seismic shaking, ground rupture, and liquefaction in the water-saturated fill of the Şuhut graben (Ergin et al., 1967).

Between 1900 and 1999, 36 earthquakes with magnitudes ranging between 4.0 and 6.8 occurred in the Akşehir–Afyon graben and its surrounding area (Koçyiğit and Özacar, 2003). The distribution of these shallow earthquake epicenters suggests that NW-trending–graben-bounding faults and a majority of the NE-trending, second-order faults are seismically active. The 26 September 1921 Argıthanı–Akşehir earthquake (M = 5.4) and the 21 February 1946 Ilgın–Argıthanı earthquake (M = 5.5), which occurred in the eastern part of the Akşehir Afyon graben, produced significant damage. However, no information on ground rupture was reported. On the other hand, in spite of the lack of reliable and accurate instrumental seismic records before 2000, these two damaging earthquakes probably originated from fault segments of the Akşehir fault zone (Koçyiğit and Özacar, 2003).

The Sultandağı earthquake of 15 December 2000 (M = 6.0, with a shallow focus of between 5.8 and 15 km) occurred at the southern margin of Eber Lake, located in the Akşehir–Afyon graben (Harvard University, 2002; Taymaz and Tan, 2001). No observation of ground rupture was made. The epicenters of the aftershocks occurred between Eber Lake and the southern margin of Akşehir Lake (Fig. 1), a 30-km-long linear seismic belt that is parallel to the southern Akşehir fault and to the northern Karagöztepe fault. It is believed that the 2000 Sultandağı earthquake ruptured part of the Akşehir fault.

Another destructive, shallow-focus (depth, 5–15 km), moderate-size earthquake (Mw = 6.5) occurred on 3 February 2002. Known as the Çay earthquake, the event occurred at the southern margin of Eber Lake, close to the epicenter of the Sultandağı event, and produced a 30-km-long rupture (Koçyiğit and Özacar, 2003). Ground surface ruptures occurred at several locations (separate earthquake fault segments) along the Akşehir fault zone, including the 200-m-long Oğuzhüyüğü rupture, with en-echelon cracks and a vertical component of 2 cm; the Çay ruptures, with 18–20 m long en-echelon open cracks spaced 2–20 m apart and with vertical displacement of 2–20 cm; and the Sultandağı ruptures about 20 km southeast of Çay, with 2000 m of closely spaced en-echelon cracks 2–4 cm long and vertical displacement of 3 cm. All ruptures were at or near the mountain front of the Sultandağı–Akşehir graben (Koçyiğit and Özacar, 2003).

The 2002 event (main shock and aftershocks) killed 42 people and injured 320. About 400 structures collapsed and another 1200 were damaged (Koçyiğit and Özacar, 2003).

Two trenches (Maltepe and Çay) were excavated to examine offsets of the 2002 Çay earthquake. The Maltepe trenches were located where 25–30 cm of vertical surface displacement was observed. These trenches revealed a total of 50 cm of vertical displacement, suggesting that an earthquake similar to the 2002 event occurred after A.D. 1150. Furthermore, an event (similar to the 2002 earthquake) with vertical displacement of 20–23 cm was observed in the Çay trench. That earthquake occurred before A.D. 760. Thus, the return period of these moderate earthquakes is thought to be about 1250 years (Akyüz et al., 2006).

Researchers have investigated the earthquakes that occurred on the Akşehir fault and its surroundings, associated with different fault segments. For example, the 1921 Doğanhisar (Ms = 5.9), 1946 Ilgın (Ms = 5.7), and 2000 Akşehir (Mw = 6.0) earthquakes have been placed on different segments (Demirtaş et al., 2002; Koçyiğit and Özacar, 2003). These earthquakes did not cause surface ruptures, and their epicenter locations are not accurately identified. While these factors lead to uncertainties regarding which segments ruptured, it is clear from the studies that moderate magnitude earthquakes such as the 2002 Çay–Eber (Afyon) earthquake should be expected in the future on other segments of the fault (Akyüz et al., 2006).

2. Methods

Tectonic geomorphology is, in part, the application of geomorphic information to tectonic processes (Keller and Pinter, 2002). The geomorphic approach in this paper utilizes a number of geomorphic

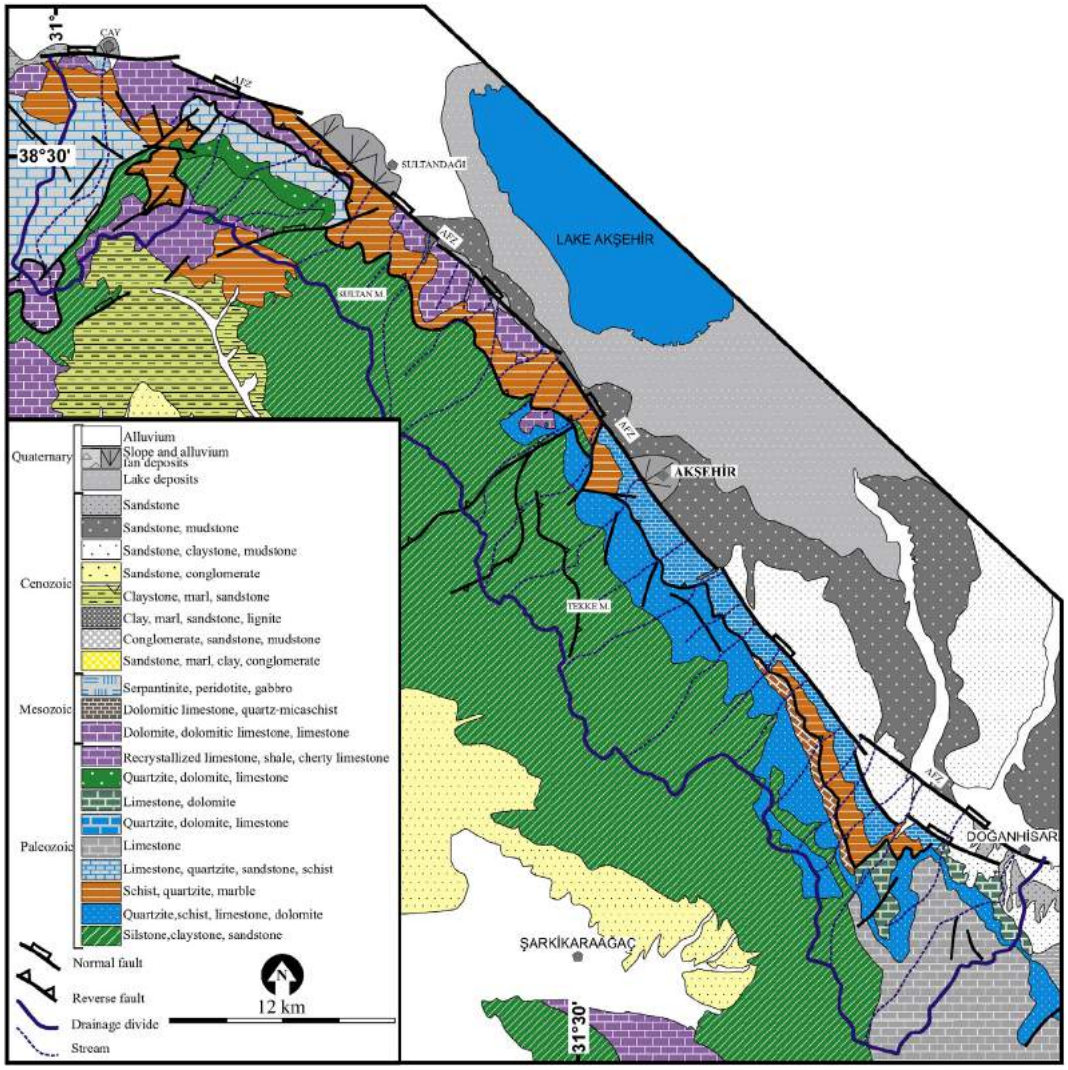

Fig. 2. Simplified geologic map of the Akşehir Sultandağı–Akşehir Horst, showing our separation of the fault into seven geomorphic fault segments. Lake Akşehir is in the adjacent Akşehir Graben. Also shown are four prominent alluvial fans from Akşehir to Cay.
Modified from Koçyiğit and Özacar (2003) and Çiçek and Koçyiğit (2009).

indices, some of which are related to mountain fronts and others to the landscape in general. In this study, we utilize 1:25,000 topographic maps and a 90-m SRTM v4.1 digital elevation model (Jarvis et al., 2008) to extract geomorphic data from which a number of the indices and general morphology may be evaluated.

Google Earth imagery was used to determine geomorphic segments of the Akşehir fault, based on linear orientation changes in the bearing of mountain fronts and areas where fronts appear to have topographic breaks or steps. This method evaluates only the geomorphic segments identified, based on the geomorphology of the front, and does not reflect earthquake segments that have been identified in recent seismic events in 2000 and 2002 (Koçyiğit and Özacar, 2003). As a result, the geomorphic segments are a rough depiction of the entire fault zone over nearly 100 km.

The Akşehir fault produces a prominent mountain front (Fig. 1C) that can be readily evaluated with a suite of geomorphic indices. Two mountain front indices, the mountain front sinuosity (S_{mf}) and the ratio of valley width to height (V_f), are typically particularly useful in the analysis of such a mountain front (Bull and McFadden, 1977; Keller and Pinter, 2002). Mountain front sinuosity is defined as the ratio of the mountain front length — as defined topographically on maps, DEMs, or aerial photographs — to the straight-line length of the mountain front:

$$S_{mf} = L_{mf}/L_s \quad (1)$$

where S_{mf} is mountain front sinuosity, L_{mf} is the length of the mountain front along the topographic break in slope at the foot of the mountain, and L_s is the straight-line length of the mountain front.

Young mountain fronts tend to have low values of S_{mf}, as they have not experienced significant range front erosion and are responding to active tectonic uplift on a relatively steep fault, keeping the front straight. On the other hand, higher values of S_{mf} reflect a more eroded front that is either older or experiencing lower rates of tectonic uplift relative to rates of erosional processes.

Valley floor width to valley height ratio, V_f, (Bull and McFadden, 1977; Keller and Pinter, 2002) can be expressed as:

$$V_f = 2V_{fw}/(E_{ld} - E_{sc}) + (E_{rd} - E_{sc}) \quad (2)$$

where V_f is the valley width to height ratio; V_{fw} is the width of the valley

floor; E_{ld} and E_{rd} are elevations of the left and right valley divides, respectively; and E_{sc} is the elevation of the valley floor.

Valley width to height ratio is measured near the mountain front and reflects the difference between incised (wineglass-shaped) valleys that are V-shaped, compared to broader U-shaped valleys (Bull and McFadden, 1977; Keller and Pinter, 2002). Low values of V_f typically are associated with higher rates of vertical tectonics along a mountain front (Keller and Pinter, 2002).

Several other geomorphic indices were selected to evaluate 32 drainage basins and facets on the northeast flank of the Sultandağı–Akşehir Horst (Figs. 1B, 3). The asymmetry factor (*AF*) was used to detect tectonic tilting that is transverse to the flow of a drainage basin (Cox, 1994); Keller and Pinter, 2002):

$$AF = 100\ (A_r/A_t) \tag{3}$$

where *AF* is the asymmetry factor, A_r is basin area to the right facing downstream, and A_t is total basin area.

Hypsometric integral (H_i) is a measure of the relative dissection of a drainage basin:

$$H_i = (m_e - mn_e/mx_e - mn_e) \tag{4}$$

where H_i is the hypsometric integral, m_e is the mean basin elevation, mn_e is the minimum basin elevation, and mx_e is the maximum basin elevation (Pike and Wilson, 1971).

Drainage basin shape (B_s) is defined as the ratio of the length of a drainage basin to its maximum width (El-Hamdouni et al., 2008). Long, narrow basins may be structurally controlled, compared to more circular basins:

$$B_s = B_l/B_w \tag{5}$$

where B_s is basin shape, B_l is basin length, and B_w is maximum basin width.

We calculated the drainage density — defined as the ratio of total lengths of all channels on a facet to the facet area of each facet along the mountain front — with the assumption that a younger facet will have a lower drainage density (see Fig. 1C for an image of channel morphology):

$$D_{df} = L_{sf}/A_f \tag{6}$$

where D_{df} is the facet drainage density, L_{sf} is the total channel length on a facet, and A_f is the area of the facet.

Facet geometry (height, width, slope, and area) and shape (triangular or trapezoidal) were measured or extracted from the DEM or from topographic maps. The distributions of facet slope, height, and bottom width were tested for normality by using the Shapiro–Wilk test (Razali and Wah, 2011). We also completed two linear regressions on facet height as the dependent variable and on facet slope and facet width as the independent variables. These regressions were performed in order to compare results with similar regressions by Tsimi and Ganas (2015).

The set of Matlab codes from the TopoToolbox (Schwanghart and Scherler, 2014) was used to extract channel profiles from a 90-m-resolution SRTM digital elevation model (DEM) (Jarvis et al., 2008). We then used two approaches to analyze the steepness of streams as proxies for active tectonics for all major basins draining the Akşehir ridge. Firstly, we calculated the steepness index k_{sn} by using the TopoToolbox (Schwanghart and Scherler, 2014) to perform a classical slope-area analysis, assuming a reference concavity of 0.45 (see Kirby and Whipple, 2012, for a review). Secondly, we calculated χ-steepness indices k_χ (see Perron and Royden, 2013; Royden and Taylor Perron, 2013) by using the set of tools developed by the Land Surface Dynamics Group at the University of Edinburgh (Mudd et al., 2014). Similarly to

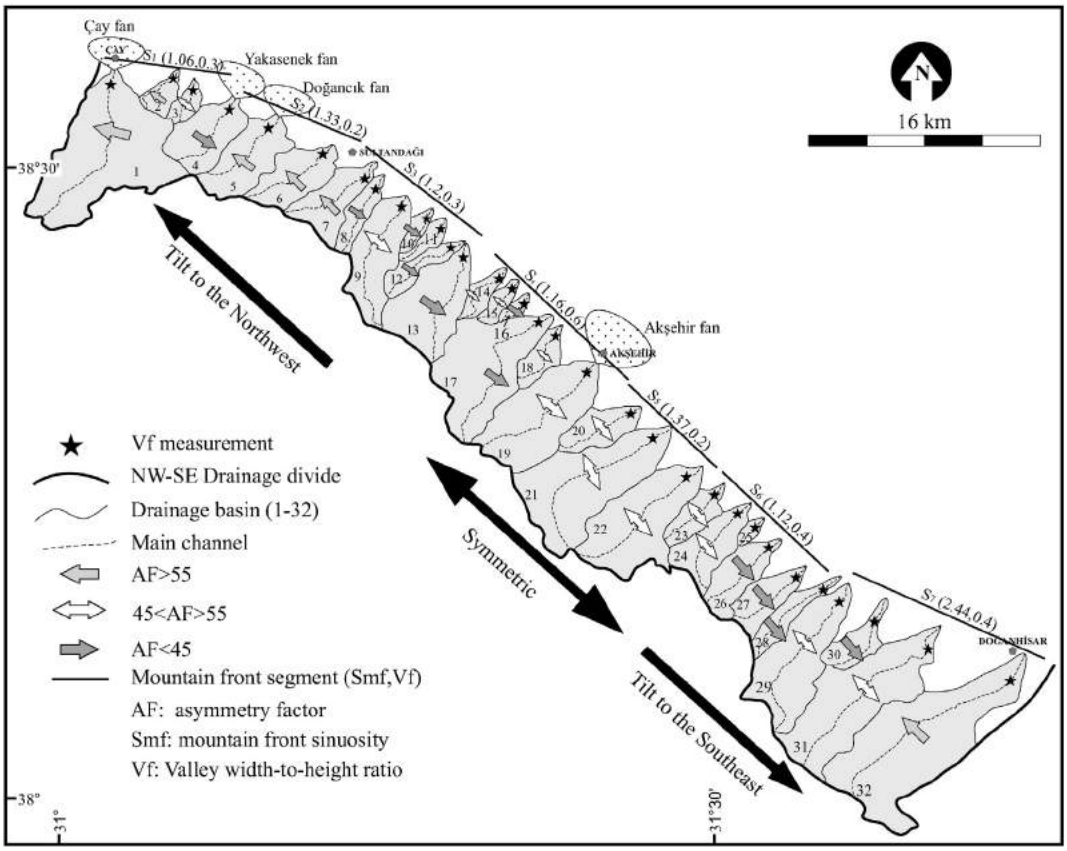

Fig. 3. Map showing the seven geomorphic segments of the Akeshir fault and values of *Vf*, *Smf*, and *AF*. Locations of alluvial fans from Akşehir to Cay are also shown.

k_{sn}, k_χ is dependent on the uplift rate, the climate, and rock properties but is less sensitive to DEM errors (Perron and Royden, 2013; Royden and Taylor Perron, 2013).

The other advantage of using k_χ is that the tools developed by the Land Surface Dynamics Group (Mudd et al., 2014) allow for a varying concavity. These tools fit linear segments to the river profile in χ-elevation space to identify changes in channel steepness and the most probable channel concavity. For a given concavity, the minimum number of segments that yield a good fit to the data are found by using maximum likelihood analysis and an Akaike information criterion (AIC). The same statistical methods are then used to find a best fit concavity. This segment-fitting algorithm can either be performed on each tributary of a channel network individually or on the combined data from an entire watershed by finding the concavity that best collapses all the tributaries onto the main stem (the collinearity test, Mudd et al., 2014). For each drainage basin, we analyzed the χ-steepness values for a reference concavity of 0.45 as well as for a 'best fit' concavity. The collinearity test has been found to identify best fit concavities well for channel networks created by numerical models but can fail in real world landscapes (Mudd et al., 2014). For that reason, we chose a mean value of the best-fit concavities for each individual tributary as the best fit concavity for the drainage basin. For each drainage basin, we first analyzed concavities ranging from 0.1 to 1 in steps of 0.05 and found the concavity with the lowest AIC value for each tributary. We then took a mean of each tributary's best fit concavity weighted by the inverse number of concavities that have AIC values within one standard deviation of the minimum AIC value. For example, if four of the 19 concavity values (between 0.1 and 1) calculated for one tributary have very similar likelihood to be the best fitting concavity (the AIC values are within one standard deviation of the minimum AIC value), then the weight assigned to the best fit concavity of the tributary in calculating the mean concavity for the entire basin would be one-fourth. On the other hand, if the minimum concavity value is well constrained and no other concavities have AIC values within one standard deviation of the minimum value, the weight of that concavity value in calculating the basin mean would be one. Any tributary with best fit concavities at the edges of the analyzed range ($\theta = 0.1$ or $\theta = 1$) was excluded from that mean. The resulting steepness values and best fit concavities are very dependent on the input parameters (Mudd et al., 2014). We performed a sensitivity analysis with varying inputs on two basins and chose our run parameters on the basis of computational efficiency, tightness of the AIC fit, and the number of tributaries that had best fit concavities >0.1 and <1. Thus, we chose an uncertainty in the elevation of 20 m, an average skip value of 1, a minimum segment length of 10, and a target length of nodes for each segment of 90 for the final analysis (Mudd et al., 2014). We also ran the entire analysis using a skip value of 2 and a minimum segment length of 20.

Tectonic tilting of the mountain front in the piedmont area was analyzed by evaluating four alluvial fans along the central and northern segments of the Sultandağı–Akşehir Horst. The method used is found in Keller and Pinter (2002). The basic principle is that tilting of alluvial fans may be identified from the topographic contours on a fan's surface. As fans tilt, the original circular contours become progressively more elliptical in shape, with their long axis oriented parallel to the direction of tilting. The magnitude of tilting may then be determined from simple mathematical analysis of the topographic shape of the contours of a particular fan (Keller and Pinter, 2002):

$$\beta = \arcsin\left((b/a)^2 \sin^2\alpha + \cos^2\alpha\right)^{0.5}) \quad (7)$$

where β is the amount of tilt in degrees; b and a are the long and short axis of the ellipse, respectively; and α is slope of the fan along the short axis of the ellipse.

Morphologic characteristics of mountain front facets were extracted from the DEM. In particular, facet shape, height, and slope were measured to examine changes in facets along the Sultandağı–Akşehir Horst (Fig. 1B). The facet geometry in this paper is defined as being composed of two basic parameters: height of the facet (H) and facet slope (Fs). Facet height calculations were performed by taking the difference between highest elevation and lowest elevation in ArcGIS. Average slope of the facet area was measured by using the zonal statistics tool in ArcGIS (Tsimi and Ganas, 2015).

The facet slope was estimated for each of 32 mountain facets, averaged for the seven geomorphic segments, and used to estimate a vertical slip rate utilizing the method of Tsimi and Ganas (2015). Tsimi and Ganas developed an empirical relationship between vertical slip rate and facet slope angle. They analyzed 232 mountain front facets using a 30-m DEM along 10 normal faults in Greece, with the vertical slip rate ranging from ~0.2–0.8 mm/y and facet slopes of 24–32°. The facets from the Greek study are steeper and have higher vertical slip rates than those found along the Akşehir mountain front. In order to extrapolate the Tsimi and Ganas (2015) relationship, these authors fit an exponential function to their data, which allowed estimation of vertical slip rates with lower facet slopes:

$$V_{sr} = 0.0328e^{0.09Fs} \quad (8)$$

where V_{sr} is the vertical slip rate, and F_s is the facet slope in degrees (Tsimi and Ganas, 2015).

3. Results

The mountain front of the Sultandağı–Akşehir Horst in the study area between Doğanhisar and Çay is ~60 km long. For the purpose of our analysis, we define seven geomorphic segments along the front

Table 1
Geomorphic indices by drainage basin number[a].

Segment	Drainage basin	S_{mf}[b]	V_f	AF	HI	Bs	Ddf
1	1	1.00	0.21	61 (−11)	0.5	2.4	1.4
1	2	1.00	0.25	80 (−30)	0.5	2.4	0.8
1	3	1.22	0.30	52 (−2)	0.4	2.6	1.2
2	4	1.13	0.20	44 (6)	0.4	2.2	0.8
2	5	1.23	0.20	66 (−16)	0.5	2.8	1.1
2	6	1.32	0.33	56 (−6)	0.6	2.6	1.2
3	7	1.10	0.41	57 (−7)	0.5	3.3	1.2
3	8	1.41	0.25	37 (13)	0.5	4.6	1.0
3	9	1.14	0.22	51 (−1)	0.5	3.9	0.9
3	10	1.09	0.38	32 (18)	0.3	3.8	1.3
3	11	1.94	0.31	47 (3)	0.6	4.0	1.0
3	12	1.07	0.26	42 (8)	0.5	4.8	0.9
3	13	2.23	0.37	27 (23)	0.5	2.1	1.2
4	14	1.75	0.37	53 (−3)	0.5	3.9	0.8
4	15	1.04	0.37	48 (2)	0.4	3.4	1.4
4	16	1.42	0.45	43 (7)	0.7	3.4	1.7
4	17	1.94	0.25	33 (17)	0.6	2.6	1.7
4	18	1.52	0.57	47 (3)	0.6	3.0	1.1
4	19	1.55	0.14	50 (0)	0.7	2.5	0.7
5	20	1.46	0.25	46 (4)	0.7	2.6	1.1
5	21	1.94	0.16	48 (2)	0.5	2.8	1.4
5	22	1.72	0.20	50 (0)	0.5	2.8	2.0
6	23	1.06	0.30	54 (−4)	0.6	3.0	1.2
6	24	1.29	0.23	47 (3)	0.6	3.0	1.5
6	25	1.15	0.30	40 (10)	0.6	2.4	1.4
6	26	1.33	0.31	44 (6)	0.6	2.7	1.6
6	27	1.91	0.47	39 (11)	0.6	2.6	1.7
6	28	1.70	0.63	44 (6)	0.5	5.9	1.5
7	29	2.43	0.68	49 (1)	0.5	4.7	1.4
7	30	1.80	0.51	37 (13)	0.3	3.0	1.3
7	31	2.71	0.30	45 (5)	0.5	3.9	0.8
7	32	3.92	0.38	59 (−9)	0.5	2.7	1.6

[a] *Smf*: mountain front sinuosity, *Vf*: ratio of valley-floor width to valley height, *AF*: drainage basin asymmetry, *HI*: hypsometric integral, *Bs*: drainage basin shape, and *Ddf*: facet drainage. Drainage basin number also refers to facet number.
[b] *Smf* values are for short lengths of the mountain front directly across a drainage at the front.

(Fig. 3). These segments are not earthquake segments, and the actual segmentation near Çay is more complex, as judged from recent earthquakes that exhibited ground deformation and ground ruptures. We used mountain front sinuosity (S_{mf}) and valley width-to-height ratio (V_f) (Fig. 3 and Table 1) to analyze the geometry of the mountain front. Of the two indices, the S_{mf} is the most informative, as it varies systematically along the Aksehir normal fault. The highest value of S_{mf} is found on the southeasternmost segment (segment 7), with a value of 2.44. To the northwest, mountain front sinuosity is generally much lower, with the lowest (1.06) value near Çay in segment 1. The valley width-to-height ratio V_f is relatively low for all segments, and drainages in all basins are deeply incised with V-shaped valleys near the mountain front. This observation suggests that less uplift is necessary to keep valleys V-shaped than to create a straight mountain front.

Mountain front facets (~100–1000 m high) are either triangular (about 80% of all facets) or trapezoidal (about 20% of all facets; see Fig. 4). Three of the seven trapezoidal facets are located along segment 2 near the northernmost part of the mountain front, while another three are located along segments 5 and 6, southeast of Akşehir (Fig. 4). Facets at the NW and SE segment ends are larger than the intervening facets, with the highest relief near Çay (Fig. 4). Steepest facets are found along the central segments, with a maximum near Akşehir (Fig. 4).

As a way of evaluating the relative dissection of the mountain front facets, we developed a new index that we call drainage density of facets (D_{df}), defined as the ratio of the total channel lengths of a particular facet divided by the area of the facet. Facet area varies from <1 to ~10 km^2, and drainage density varies from ~0.7 to 2.0 km^{-1} (Table 1). Two-thirds of the values of D_{df} are <1.5. The facets in general have a remarkably low drainage density, and most drainage appear to be rill-like, nearly straight, steep channels that reflect the youthfulness of the facet dissection and the high rock strength. The segment-averaged drainage density of the facets is higher in segments 4–7 than in 1–3, with a maximum in segments 5 and 6.

We analyzed three geomorphic indices of drainage basins (Table 1). These are the drainage basin shape (B_s), the hypsometric integral (H_i), and the channel steepness (k_{sn} and k_χ). The index B_s is basically a measure of how elongated drainage basins are. Values of B_s vary from ~2 to 3 (Table 1), suggesting that the drainage basins emerging from the base of the uplift are long and narrow and indicative of relatively recent high rates of tectonic activity.

The hypsometric integral (H_i) has been utilized in many studies as a measure of the relative topographic development and as a surrogate for the age of a basin (Keller and Pinter, 2002). High values of this index are suggestive of younger geomorphic surfaces, while lower values are suggestive of more long-term erosion, with a greater portion of the

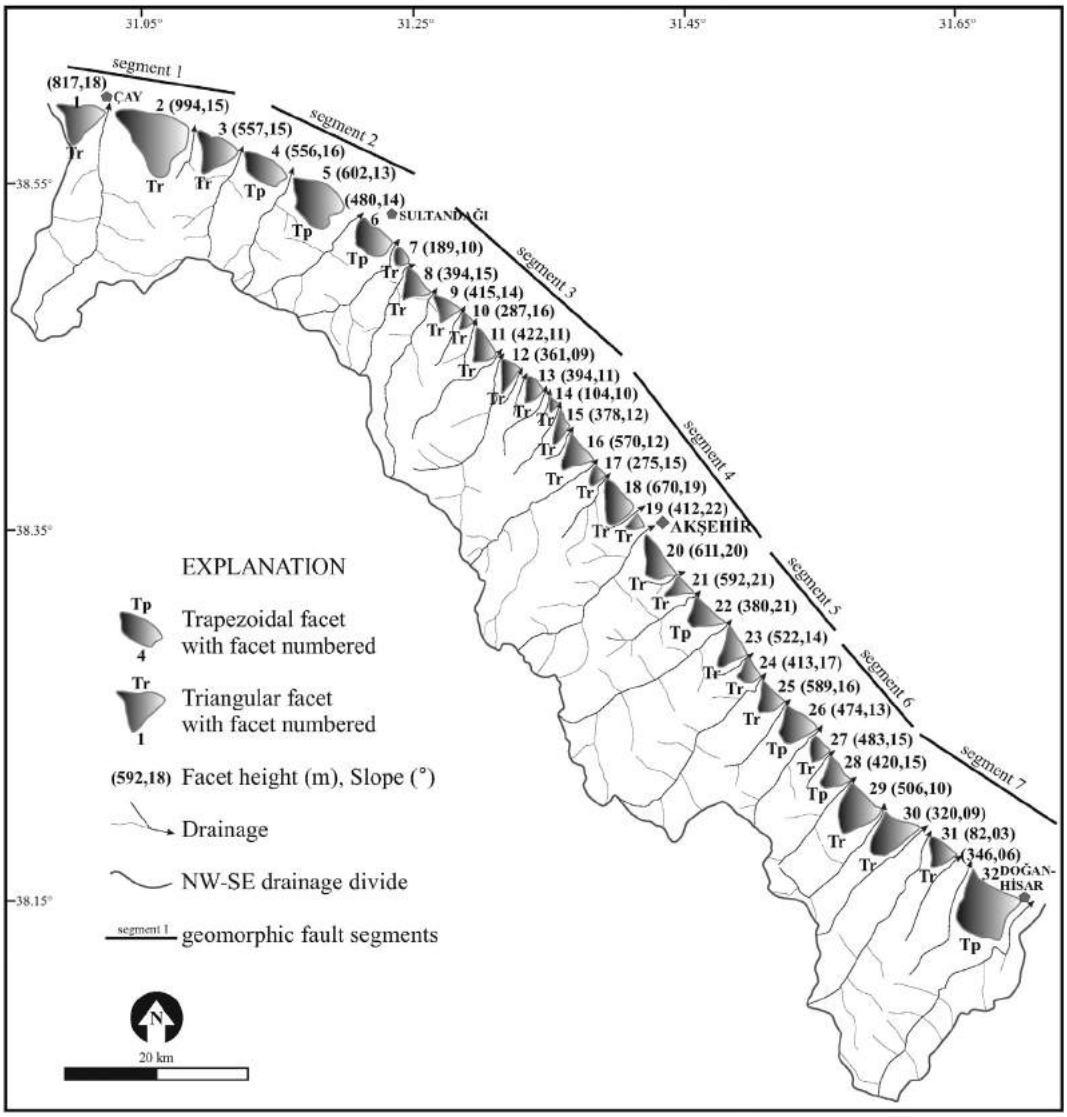

Fig. 4. Map showing facet shapes and values of facet height and slope.

Table 2
Tilt of alluvial fans[a].

Fans	A (km)	B (km)	α (°)	β (°)
Çay	6.5	5.3	0.9	0.38 to the south
Yakasenek	6.3	6.1	1.92	0.20 to the southwest
Dogancik	6.5	5.5	1.67	0.58 to the southwest
Akşehir	10	8.9	1.22	0.45 to the southwest

[a] For location of alluvial fans, see Fig. 3.

topography being at relatively low elevations. Eighty-four percent of H_i values are 0.5–0.7, and 38% of the values are 0.6–0.7 (Table 1). The highest values of 0.7 are in segments 4 and 5 (central segments) (Table 1). These H_i values are not particularly useful in delineating details of change along the mountain uplift, but the relatively high values, >0.6, are suggestive of recent topographic development. The values also suggest that much of the erosional development may be close to an equilibrium between uplift and erosion that is probably achieved relatively quickly in the topographic development of a landscape.

Results of the asymmetry factor (*AF*) that we used to detect tectonic tilting transverse to the flow of a drainage basin (Cox, 1994; Keller and Pinter, 2002) vary from 27 (tectonic tilting to the right side of the basin — i.e., the southeast) to 80 (tectonic tilting to the left side of the basin — i.e., the northwest), and an overall trend is apparent (Fig. 3, Table 1). A tendency for tilt to the southeast for segments 6 and 7 and to the northwest for segments 1 and 2 was noted, while basins in the central segments (4 and 5) tend to be symmetric and show no preferred tilt direction. Our interpretation of this pattern of asymmetry is that the morphology of the long, linear, Z-shaped horst block, while geomorphically segmented, is roughly biconvex lens-shaped (see Jackson and Leeder, 1994). The northwestern corner is complicated by the Outer Isparta Angle where domal uplift and radial extension occur (Koçyiğit and Özacar, 2003).

Several prominent alluvial fans exist along the uplifted block adjacent to the central and northwestern segments (segments 1–4). The fans are all back-tilted toward the mountain front, as is expected for most normal faults (Table 2) (Jackson and White, 1989).

Most stream profiles of the major watersheds draining the Akşehir Horst block show strong deviations from an ideal concave profile (Fig. 5A). Major knickpoints are apparent, especially for streams along the central part of the fault. In some southeastern rivers, broad convex profiles occur rather than discrete knickpoints (Fig. 5A). For basins 7, 19, 21, 22, and 26, steepening occurs at the boundary between weaker silt/sandstone and stronger quartzite, schist, limestone, or dolomite.

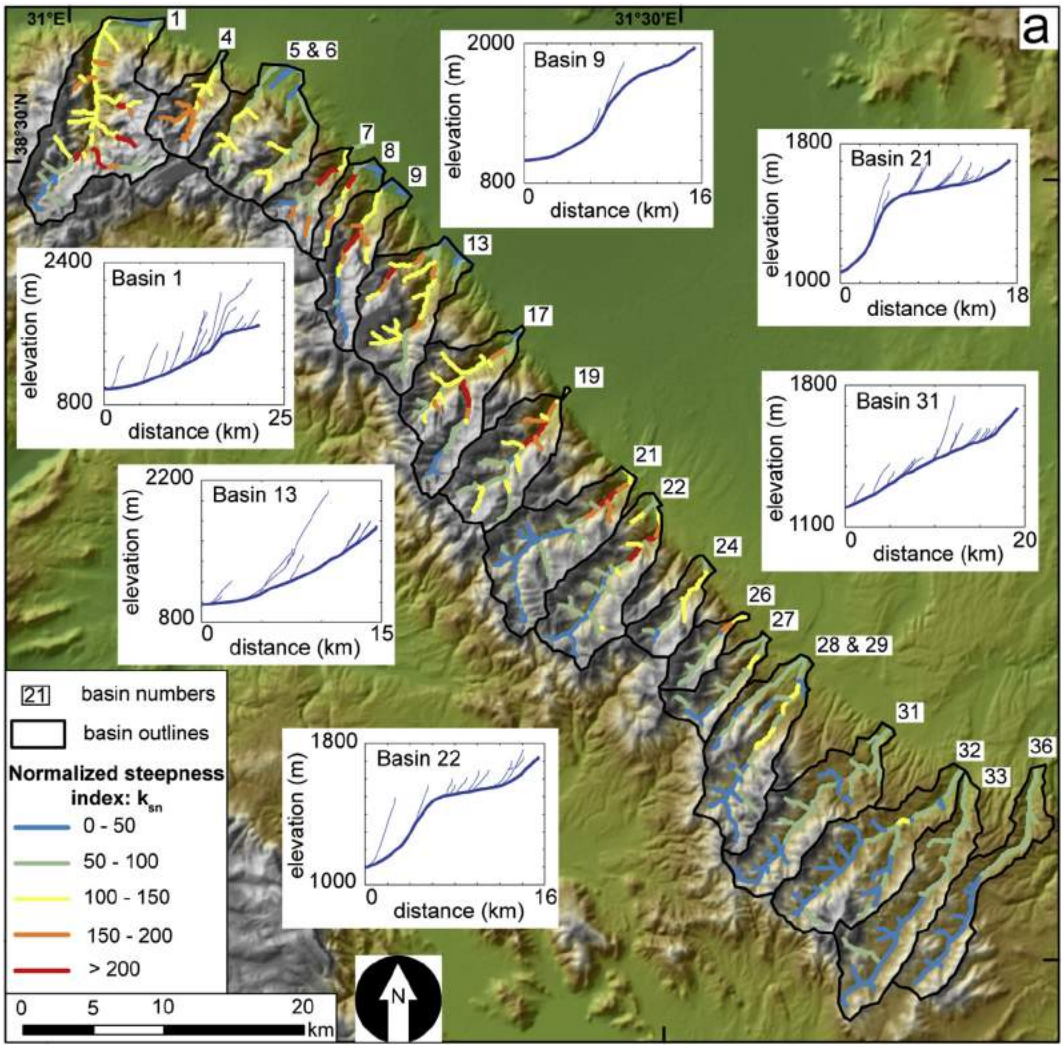

Fig. 5. Results from (A) classic k_{sn} analysis, assuming a reference concavity of 0.45 and (B) χ-steepness analysis. Only major basins were analyzed, and two more basins to the south were included to show the trend of decreasing steepness to the south. In the stream profile plots, the trunk stream is marked with a thick blue line and tributaries with thin blue lines. Distances are measured along the stream from the mouth of the channel. Note that high values of steepness indices on the downstream ends of basins 7, 19, 21, 22, and 26 are probably lithologically controlled. Therefore, the steepness values along the entire stream should be considered. Basin 8 did not yield a result in the χ-analysis and is ignored here.

For other knickpoints, a lithological control is not apparent, and these convexities are interpreted as resulting from uplift at the mountain front (Kirby and Whipple, 2012)

These complicated channel profiles render the assumptions behind the classical k_{sn} approach problematic, and a segment-fitting algorithm allowing for variable concavities promises better results. Within each catchment, 0–25% of tributaries have best fit concavities at the boundaries of the analyzed range (0.1–1) and are excluded from the analysis. Running the χ-analysis with different input parameters shows that for most (not all) basins, a higher minimum length of channel segments results in a tighter fit with fewer AIC values within one standard deviation of the minimum AIC value. However, more basins have to be excluded from the analysis because $\theta = 0.1$ or $\theta = 1$. Increasing the number of nodes in a segment up to 110 and 120 does not improve the fit significantly (at least for the two basins that we used for the sensitivity analysis) but becomes computationally very costly. For basin 8, all three tributaries yielded $\theta = 0.1$, so we chose to ignore this basin in the χ-analysis.

Normalized steepness indices (Fig. 5A) and χ-steepness indices (Fig. 5B) show a similar pattern of high values in the north (basins 19 and north) and lower values for the southernmost basins (28 and south). This pattern is not limited to major knickzones but is apparent within the entire watershed. The K_{sn} values are generally 1.5–4 times higher in the north than in the south, and the χ-steepness indices are up to one order of magnitude higher. For the central basins (21–27), the data are ambiguous. Whereas k_{sn} values are low in these basins, with steepening restricted to lithologically controlled knickpoints on the downstream end of the channels (Fig. 5A), the χ-steepness indices are higher here than in the southern basins (Fig. 5B). We note that when a reference concavity of 0.45 instead of the best-fit concavities is assumed in the χ-analysis, the pattern, as well as the relative magnitudes of χ-steepness values, are similar to the k_{sn} values. We further note that if we choose a mean skip value of 2 and a minimum segment length of 20 for the χ-analysis, the overall pattern of χ-steepness indices is very similar to the one presented here, except for pushing the boundary between steep and gentle streams from basin 27 northward to basin 22. Contoured values of χ-steepness, interpolated by using a natural neighbor algorithm, illustrate the pattern of very high steepness in the north, medium to high steepness in the central segments, and low steepness in the south (Fig. 6). Extreme values around basins 7–9, 21, 22, and 26 are probably controlled by lithology. The broad pattern of stream steepness agrees well with the pattern of relatively low mountain front sinuosity and steep facets in the northern and central segments. We interpret this consistent spatial pattern of geomorphic indices as reflecting northward-increasing uplift rates along the Akşehir normal fault.

Vertical rates of uplift were estimated for the seven mountain front segments, using the method of Tsimi and Ganas (2015). The rates vary from about 0.06 ± 0.05 m/ky at the southern end of the structure (segment 7) to 0.23 ± 0.05 m/ky (segment 5 in the central part of the structure) and 0.16 ± 0.05 m/ky at the northwestern end of the structure (segment 1; Fig. 7 and Table 3). Apparently consistent with the trend

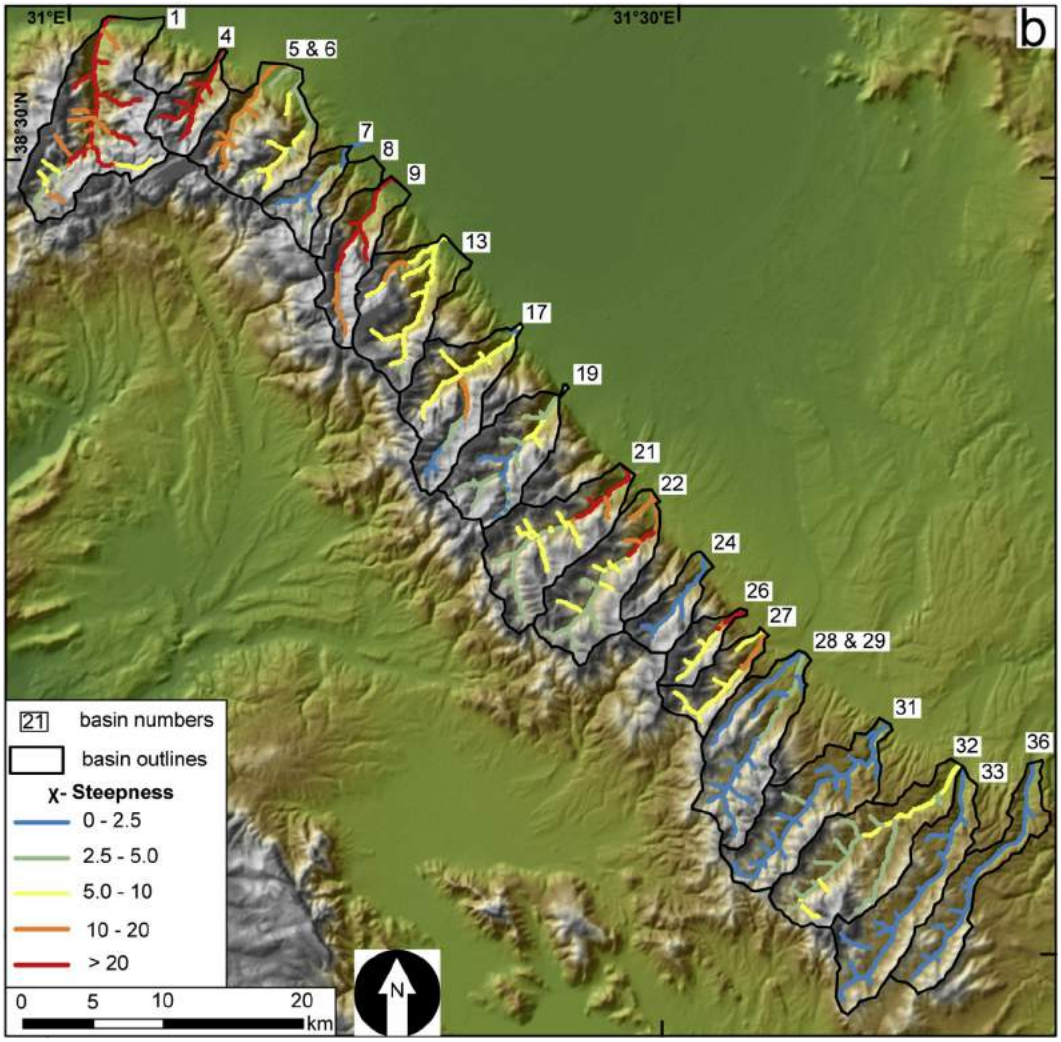

Fig. 5 (*continued*).

of other geomorphic indices, the northern and central parts of the structure have recently been uplifting at a higher rate than the southern segments, with highest rates in the central part of the Akşehir fault. Vertical slip rate of the Akşehir fault since the late Pleiocene was estimated to be 0.3 m/ky (Koçyiğit and Özacar, 2003). Thus, the estimated rates of uplift based on facet slope are a little lower but of the same order of magnitude than the estimated late Pliocene and early Pleistocene rates.

The Shapiro–Wilk test for normality suggests that the distribution of facet slopes and height is normally distributed at the 5% significance level, while facet width at the base is not. Linear regression on facet height as the dependent variable and facet slope as the independent variable (n = 32) yields an r^2 of 0.25. Linear regression of facet height as the dependent variable and facet base width as the independent variable (n = 32) has an r^2 of 0.52. These r^2 values are very similar to those reported by Tsimi and Ganas (2015) for the same regressions (0.25 and 0.44, respectively for n = 232). Thus, the regression analysis suggests that the same amount of variability of the facet height can be explained by the variability of facet slope and facet base width in both study areas (Greece and Turkey). Assuming that the facet height is a measure of the height of an eroded fault scarp and that the deduced vertical slip rates are about right, the oldest segment (S7) is about 8 Ma and the youngest (S5) is about 3 Ma. The other segments are about 4–6 Ma (Table 4). Thus, the Akşehir fault initiated in the late Miocene to early Pliocene and remains active today. These estimates are very speculative but are coincident with estimates of onset or at least acceleration of extension in eastern Turkey around the Pliocene (Jackson, 1994).

4. Discussion

While our estimates of vertical slip rates for the Akşehir fault are consistent with the geologic rates and the pattern of geomorphic indices, they are obtained by extrapolating the fit of Tsimi and Ganas (2015) to lower slopes. Furthermore, we use a 90-m DEM, whereas Tsimi and Ganas (2015) used a 30-m DEM. Measured topographic slope may vary with DEM resolution used (Kienzel, 2004), and as a result, the estimated vertical slip rate is probably a minimum. We calculated average facet slope from 1:25,000 topographic maps and compared the slope values with those from the 90-m DEM. Of the 32 facets, 14 facets had the same slope, 16 varied by 1°, and 2 by 2°. Thus, the 90-m DEM apparently provides reliable values of average facet slope.

Because only segment 5 has facet slopes close to the ones used by Tsimi and Ganas (see Fig.7), we need to extrapolate their regression to lower values. As an alternative, we could use the relationship between vertical uplift rate and facet height (r^2 of 0.63) derived for a large data set of 100–550 m high facets in the Basin and Range (DePolo and Anderson, 2000). Applying this regression to the facets along the Akşehir fault would predict (with the exception of segment 7) significantly higher vertical slip rates and younger ages for the Akşehir normal fault. We prefer the slip rates deduced using facet slope (Tsimi and Ganas, 2015) for the following reasons, but we acknowledge that these rates are likely minimum estimates. Tsimi and Ganas (2015) reported a weak statistical relationship (r^2 of 0.33) between facet height

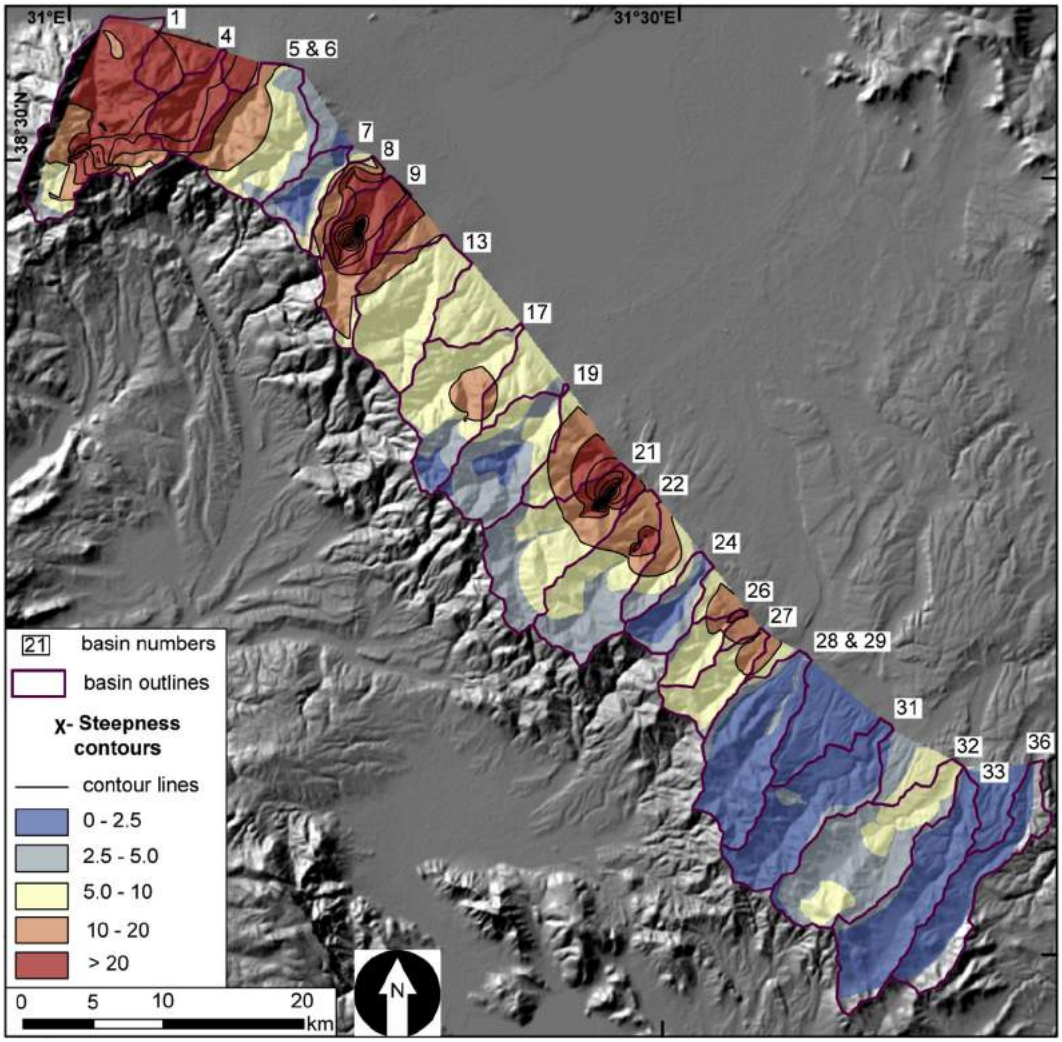

Fig. 6. Contoured values of χ-steepness. Note that the high values in the central segment are probably lithologically controlled.

and vertical slip rate. Differences in the ability of statistical relations to predict slip rate from scarp height may be related to how facet height is measured, although other more complex reasons involving tectonic framework, rock types, and climate, may be factors. Furthermore, about 50% of the variation of facet height could be explained with variations of facet base length (Tsimi and Ganas, 2015, and this study), and the relationship between base length and slip rate is not obvious. Finally, the Great Basin has a significantly different climate and a different tectonic framework, with lower rates of extension (Dickinson, 2002) compared to the southwest of Turkey (see Le Pichon et al., 1995; Reilinger et al., 2000), while the tectonics and climate of Greece are more similar (Jackson, 1994; Tsimi and Ganas, 2015).

We tested the hypothesis that facet slope decreases with time in order to continue a discussion initiated by Wallace (1978) who asked how long facets may remain in the landscape as recognizable topographic features. Linear regression with the dependent variable (Y) as average slope in degrees and independent variable (X) as the age of the facet yields the best linear fit ($Y = 23.7–1.8X$; r^2 is 0.59). Thus, excluding facet 1 where domal uplift is occurring, the oldest facet (8.4 My, segment 7) has the lowest facet slope (7°), and the youngest facet (2.7 My, segment 5) has the highest facet slope (21°). The remainder of the facets have ages of 4–6 My and facet slopes of 12–15° (Fig. 4 and Table 3). Assuming facet slopes all started at about 60°, a linear rate of scarp slope decline consistent with this data set would be about 7° per million years. The rate of slope decline is probably not linear (Wallace, 1978), being much greater earlier in the history of facet development and then slowing down. Thus, for a scarp that forms in a relatively short time, the facet could be consumed by erosion in about 10 My. This apparently is what is happening to segment 7. Note that the above argument does not suggest that slip rates change with time, even though the slopes change through time. Rather, the decline of facet slope with age suggests that a correction for the decline of slope with facet age should ideally be taken into consideration when calculating slip rates from facet slopes. However, given the variability of erosion rates and facet morphologies with rock type, climate, and slip rates, an attempt to correct for slope decline is unlikely to improve our simple approach. Rather, we acknowledge that our analysis is approximate but seems to accurately capture the broad patterns in the region. More facet chronology is necessary to adequately answer the question of facet antiquity and persistence in the landscape.

Similarly, the broad brush approach to the steepness analysis of rivers merits skepticism, and a more careful and formal inversion may yield better insights. However, for the purpose of this study, the shapes of the river profiles seem to clearly confirm the pattern we see from other indices with steeper rivers and thus (interpreted) higher uplift rates in the north and slower uplift rates in the south. For example, values of mountain front sinuosity for segment 7 are about two times greater (reflecting the much more sinuous front) than other segments, while steepness values k_χ and k_{sn} for this segment are 2–10 times lower than in the north. Steepness values along the central section of the Akşehir block are less clearly resolved, although we favor the results from the χ-analysis that allow for a varying concavity and support relatively higher uplift rates north of basin 22 or even 27.

Evolution of mountain front facets along a normal fault uplift can be complex. Wallace (1978) presented a simple model that substituted space for time, which we revised slightly to include selected geomorphic indices (Fig. 8). We also show a similar model for trapezoidal facets (Fig. 9). Both models assume that facets are eroded fault scarps. The evolutionary approach in Figs. 8 and 9 is decidedly Davisian, that is, cyclic with emphasis on structure, process, and stage (age) (Davis, 1899). Models in Figs. 8 and 9 are time dependent, and Time 1 to Time 3 in

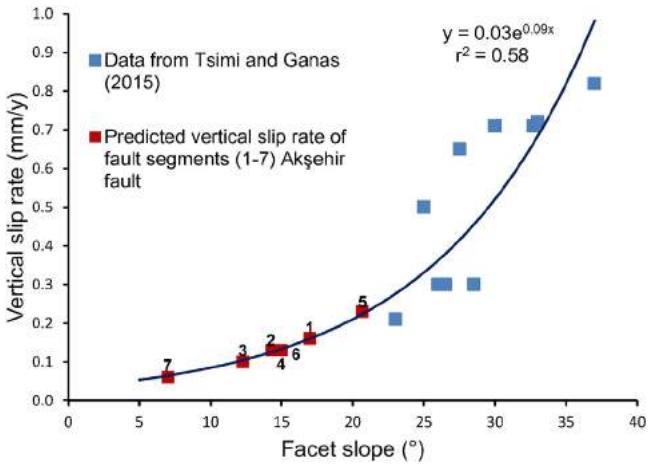

Fig. 7. Exponential relationship between facet slope and vertical slip rate, showing data from Tsimi and Ganas (2015) (blue) and facet slopes along segments of the Akşehir fault. Predicted values of the vertical slip rate are probably minima (cf. text for more detail).

Table 3
Facets and vertical slip rates.

Segment	Facet number	Facet slope (°)	Average facet slope by segment (°)		Predicted vertical slip rate (mm/y)[a]
1	1	18		Segment 1	
1	2	15	16.98		0.16
1	3	15			
2	4	16		Segment 2	
2	5	13	14.33		0.13
2	6	14			
3	7	10		Segment 3	
3	8	15	12.30		0.10
3	9	14			
3	10	16			
3	11	11			
3	12	9			
3	13	11			
4	14	10		Segment 4	
4	15	12	15.00		0.13
4	16	12			
4	17	15			
4	18	19			
4	19	22			
5	20	20		Segment 5	
5	21	21	20.66		0.23
5	22	21			
6	23	14		Segment 6	
6	24	17	15.00		0.13
6	25	16			
6	26	13			
6	27	15			
6	28	15			
7	29	10		Segment 7	
7	30	9	7.00		0.06
7	31	3			
7	32	6			

[a] Vertical slip predicted by equation of Tsimi and Ganas, 2015. $y = 0.0328e^{0.0938x}$, $r^2 = 0.58$.

Table 4
Estimated age of fault segments based on maximum facet height and estimated vertical slip rate.

Segment	Height of highest facet (m)	Vertical slip rate (m/ka)	Age of segment (ma)[a]
1	994	0.16	6.2
2	602	0.13	4.6
3	422	0.10	4.2
4	670	0.13	5.2
5	611	0.23	2.7
6	589	0.13	4.5
7	506	0.06	8.4

[a] Age assumes facets are eroded fault scarps.

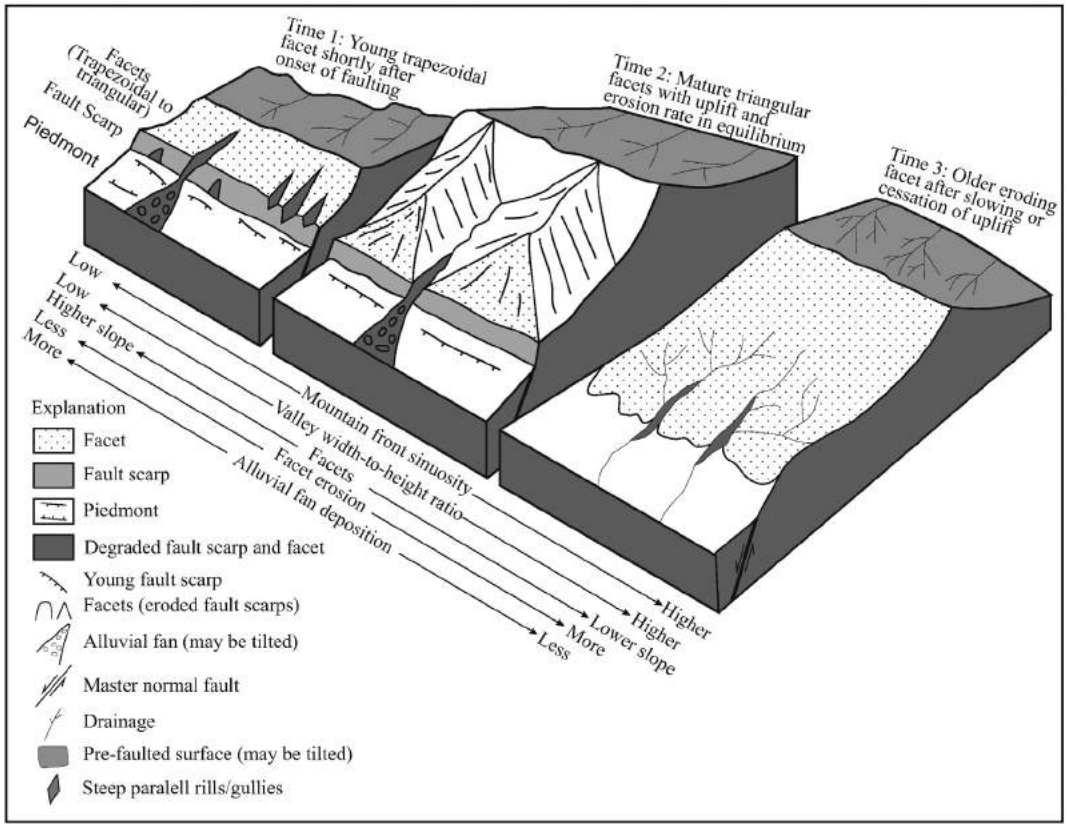

Fig. 8. Idealized diagram of triangular facet development over relative time, using generalized concepts of variability of mountain front and facet characteristics measured in this study. Modified and inspired after Wallace (1978).

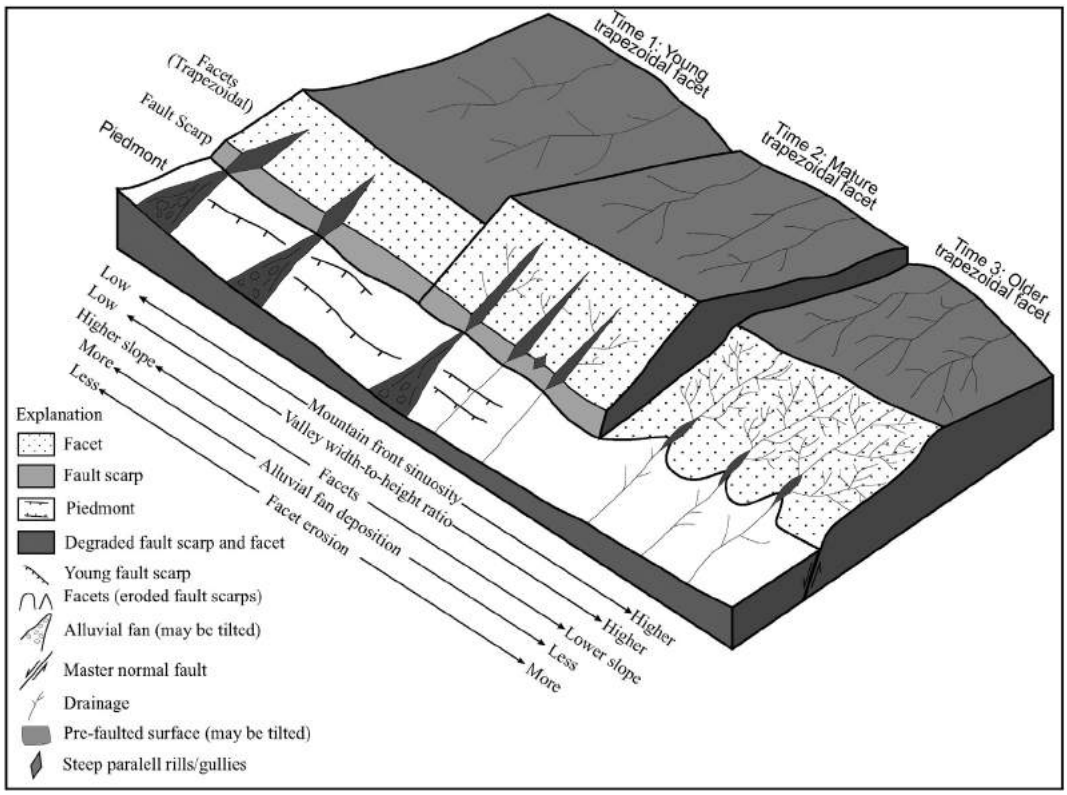

Fig. 9. Idealized diagram of trapezoidal facet development over relative time, using generalized concepts of variability of mountain front and facet characteristics measured in this study. Modified and inspired after Wallace (1978).

Figs. 8 and 9 represent geomorphic change through time of facet development. For stage Time 3 in Fig. 8 to be reached, we assume that uplift rate eventually decreases with time and that erosion continues to produce wide, relatively low relief piedmonts. Figs. 8 and 9 show some of the changes of geomorphic form and values of mountain front indices we observe in this study. However, this Davisian approach, while having the advantage of simplicity and usefulness for discussion, can be criticized for not paying sufficient attention to process (virtually nothing is known about the erosion rate, role of deposition on the piedmont, and links of both to uplift rates). Furthermore, the evolution of the Akşehir fault and the Sultandağı–Akşehir Horst is considerably more complex than the simple models presented here. Fault segments have propagated laterally, and uplift varies from segment to segment. That being said, the models are useful for discussion purposes and for the general understanding of potential changes in facet form with time.

The transformation of a young trapezoidal facet to an older triangular facet depends on rock resistance, climate, slope processes (erosion and deposition), and rate of faulting that generates the mountain front. Initially, steep channels with slot morphologies are bordered by trapezoidal facets. Canyons on both sides of a facet may widen by slope processes, such as erosion by mass movements, and with time form more triangular-shaped facets and adjacent wineglass-shaped, cross-valley morphologies. Facets may remain trapezoidal if slot canyons persist because of high uplift rates and the presence of resistant rocks in the footwall.

Eighty percent of the facets are triangular and 20% are trapezoidal. A triangular form can naturally develop (replace a trapezoidal form) if bounding streams erode and widen. Features that could be interpreted as tectonic benches (not investigated in this research) are present along the mountain front, usually high above the base of the front. We note that six out of seven trapezoidal facets occur on the more rapidly deforming segments that have potentially seen a more recent development; their position along the fault is, therefore, consistent with a model of scarp development from younger trapezoidal to older triangular. However, the large trapezoidal facet in segment 7 does not fit into this model. Overall, the use of facet shape to estimate the age of a mountain front is not without ambiguity, and several geomorphic indices should be combined to yield an average pattern of mountain front evolution.

The Akşehir fault presents a serious earthquake hazard, and the region has a history of many moderate to large earthquakes. Two moderate events of M 6 and 6.5 occurred in 2000 and 2002, respectively. Most likely, future events will be moderate but damaging M 6 to 6.5 earthquakes, based on segment lengths (10–15 km). Facets (segments 4 and 5) near Akşehir, in the central part of the fault, are steepest and have the highest vertical slip rates. As a result, the tectonic geomorphology suggests that the frequency of M6 earthquakes can be expected to be higher along this young part of the fault than to the southeast. Segment 1, because of recent earthquake activity and the unique tectonic setting of the Outer Isparta Angle, is also likely to continue to produce moderate earthquakes. If several or all of the fault segments ruptured together along a length of 50–60 km, a larger event of M 6.5 to 7.5 is possible (Wells and Coppersmith, 1994).

5. Conclusions

We conclude that:

- The active Akşehir fault has produced a linear mountain front and that the analysis of several geomorphic indices suggests that the central and northern segments are more active than the southern segment.
- Estimated rates of vertical slip have significant uncertainties, but they range from 0.06 to 0.23 m/ky, with the highest values in the northern six segments.
- Estimated ages of the seven segments vary (with significant uncertainty of ±2 Ma) from about 8 to 3 Ma, with most being 4 to 6 Ma. Thus, the fault and uplift started in the late Miocene-early Pliocene and continues to the present.
- The Akşehir fault continues to present a serious seismic earthquake hazard, with moderate M 6–6.5 events expected to occur every 1000 years and the possibility for earthquakes with magnitudes up to 7.5.

Acknowledgments

We gratefully acknowledge the constructive criticism and suggestions for improvement by William B. Bull, Athanassios Ganas, and two unknown reviewers. Richard Marston and Bill Norrington edited the entire manuscript and provided useful suggestions.

References

Akyüz, H.S., Uçarkuş, G., Şatır, D., Dikbaş, A., Kozacı, Ö., 2006. 3 Şubat 2002 Çay depreminde meydana gelen yüzey kırığı üzerinde paleosismolojik araştırmalar. Yerbilimleri 27, 41–52.
Blackwelder, E., 1928. The recognition of fault scarps. J. Geol. 36, 289–311.
Bull, W.B., 2007. Tectonic Geomorphology of Mountains: A New Approach to Paleosiesmology. Blackwell publishing, MA.
Bull, W.B., McFadden, L.D., 1977. Tectonic geomorphology north and south of the Garlock fault, California. In: Doehering, D.O. (Ed.), Geomorphology in Arid RegionsProceedings at the Eighth Annual Geomorphology Symposium. State University of New York, Binghamton, NY, pp. 115–138.
Burbank, D.W., Anderson, R.S., 2012. Tectonic Geomorphology. second ed. Wiley-Blackwell (454 pp.).
Çiçek, A., Koçyiğit, A., 2009. A NNE-trending active graben in the Isparta Angle, SW Turkey: Karamık Graben, its geometry, age and earthquake potential. Trabajos de Geología, Universidad de Oviedo 29, 168–174.
Cox, R.T., 1994. Analysis of drainage-basin symmetry as a rapid technique to identify areas of possible Quaternary tilt-block tectonics: an example from the Mississippi Embayment. Geol. Soc. Am. Bull. 106, 571–581.
Davis, W.M., 1899. The geographical cycle. Geogr. J. 14, 481–504.
Davis, W.M., 1903. The mountain ranges of the Great Basin. Bulletin of the Museum of Comparative Zoology. 42, pp. 129–177.
Demirtaş, R., Iravul, Y., Yaman, M., 2002. 03 Şubat 2002. Eber ve Çay depremleri. AlGM-DAD raporu, http://sismo.deprem.gov.tr/deprem/depremraporlari/eberson.pdf.
DePolo, C.M., Anderson, J.G., 2000. Estimating the slip rates of normal faults in the Great Basin, USA. Basin Res. 12, 227–240.
Dickinson, W.R., 2002. The basin and range as a composite extensional domain. Int. Geol. Rev. 44, 1–38.
El-Hamdouni, R., Irigaray, C., Fernandez, T., Chacón, J., Keller, E.A., 2008. Assessment of relative active tectonics, southwest border of Sierra Nevada (southern Spain). Geomorphology 96, 150–173.
Emre, O., Duman, T., Dogan, A., Ozalp, S., Tokay, F., Kuscu, I., 2003. Surface faulting associated with the Sultandagi earthquake (Mw 6.5) of 3 February 2002, southwestern Turkey. Seismol. Res. Lett. 74, 382–392.
Ergin, K., Gulco, U., Uz, Z., 1967. Türkiye Ve Civarının Deprem Kataloğu (Milattan Sonra 11 yılından 1964 Sonuna Kadar): An Earthquake Catalogue for Turkey and its Environs (11 BC to the End of 1964). Istanbul Technical University, Faculty of Mines, Department of Geophysical Engineering Publication (in Turkish).
Gilbert, G.K., 1928. Studies of basin and range structures. U.S. Geological Survey Professional Paper. 153 (92 pp.).
Harvard University, 2002. http://www.seismology.harvard.edu.
Jackson, J., 1994. Active tectonics of the Aegean region. Annu. Rev. Earth Planet. Sci. 22, 239–271.
Jackson, J., Leeder, M., 1994. Drainage systems and the development of normal faults: an example from Pleasant Valley, Nevada. J. Struct. Geol. 16, 1041–1059.
Jackson, J., White, N., 1989. Normal faulting in the upper continental crust: observations from regions of active extension. J. Struct. Geol. 11, 15–36.
Jarvis, A., Reuter, H.I., Nelson, A., Guevara, E., 2008. Hole-filled SRTM for the globe Version 4. Available from the CGIAR-CSI SRTM 90 m Database (http://srtm.csi.cgiar.org).
Keller, E.A., Pinter, N., 2002. Active Tectonics: Earthquakes, Uplift and Landscapes. second ed. New Jersey, Prentice Hall (338 pp.).
Keyes, C.R., 1909. Lineaments of the desert. Popular Science Monthly 74, 19–30.
Kienzel, S., 2004. The effect of DEM raster resolution on first order, second order and compound and terrain derivatives. Trans. GIS 8, 83–111.
Kirby, E., Whipple, K.X., 2012. Expression of active tectonics in erosional landscapes. J. Struct. Geol. 44, 54–75.
Koçyiğit, A., Deveci, S., 2007. A N-S-trending active extensional structure, the Şuhut (Afyon) graben: commencement age of the extensional neotectonic period in the Isparta Angle, SW Turkey. Turk. J. Earth Sci. 16, 391–416.
Koçyiğit, A., Özacar, A.A., 2003. Extensional neotectonic regime through the NE Edge of the outer Isparta Angle, SW Turkey: new field and seismic data. Turkish J. Earth Sci. 12, 67–90.
Koçyigit, A., Gürboga, S., Kalafat, D., 2013. Nature and onset age of neotectonic regime in the northern core of Isparta Angle, SW Turkey. Geodinamica Acta 25, 52–85. http://dx.doi.org/10.1080/09853111.2013.839126.

Le Pichon, X., Chamot-Rooke, N., Lallemant, S., Noomen, R., Veis, G., 1995. Geodetic determination of the kinematics of Central Greece with respect to Europe: implications for eastern Mediterranean tectonics. J. Geophys. Res. 100, 12,675–12,690.
Louderback, G.D., 1904. Basin-range structures of the Humboldt region. Geol. Soc. Am. Bull. 15, 289–346.
Menges, C.M., 1990. Late Cenozoic rift tectonics and mountain-front landforms of the Sangre de Cristo Mountains near Taos, northern New Mexico. New Mexico Geological Society Guidebook. 41st Field Conference, pp. 113–122.
Mudd, S.M., Attal, M., Milodowski, D.T., Grieve, S.W.D., Valters, D.A., 2014. A statistical framework to quantify spatial variation in channel gradients using the integral method of channel profile analysis. J. Geophys. Res. Earth Surf. 119 (2) (p. 2013JF002981).
Özer, N., 2006. New information on earthquake history of the Akşehir–Afyon Graben System, Turkey, since the second half of 18th century. Nat. Hazards Earth Syst. Sci. 6, 1017–1023.
Perron, J.T., Royden, L., 2013. An integral approach to bedrock river profile analysis. Earth Surf. Process. Landf. 38 (6), 570–576.
Pike, R.J., Wilson, S.E., 1971. Elevation-relief ratio, hypsometric integral and geomorphic area-altitude analysis. Geol. Soc. Am. Bull. 82, 1079–1083.
Piper, J.D.A., Gürsoy, H., Tatar, O., İşseven, T., Koçyiğit, A., 2002. Paleomagnetic evidence for the Gondwanic origin of the Taurides and rotation of the Isparta Angle, southern Turkey. Geol. J. 37, 317–336.
Razali, N.M., Wah, Y.B., 2011. Power comparisons of Shapiro–Wilk, Kolmogorov–Smirnov, Lilliefors and Anderson–Darling tests. J. Stat. Model. Analytics 2, 21–33.
Reilinger, R.E., Ergintav, S., Burgmann, R., McClusky, S., Lenk, O., Barka, A., Gurkan, O., Hearn, L., Feigl, K.L., Cakmak, R., Aktug, B., Ozener, H., Toksoz, M.N., 2000. Coseismic and postseismic fault slip for the 17 August 1999, M = 7.5, Izmit, Turkey earthquake. Science 289 (5484), 1519–1524.
Royden, L., Taylor Perron, J., 2013. Solutions of the stream power equation and application to the evolution of river longitudinal profiles. J. Geophys. Res. Earth Surf. 118 (2), 497–518.
Schwanghart, W., Scherler, D., 2014. Short communication: TopoToolbox 2 — MATLAB-based software for topographic analysis and modeling in earth surface sciences. Earth Surf. Dynam. 2 (1), 1–7.
Taymaz, T., Tan, O., 2001. Source parameters of June 6, 2000 Orta–Çankiri (Mw = 6.0) and December 15, 2000 Sultanda–Akflehir (Mw = 6.0) earthquakes obtained from inversion of teleseismic P- and SH-body-waveforms. Symposia on Seismotectonics of the North-Western Anatolia-Aegean and Recent Turkish Earthquakes, Istanbul, Extended Abstracts, 96–107.
Ten Veen, J.H., 2004. Extension of Hellenic forearc shear zones in SW Turkey: the Pliocene-Quaternary deformation of the Eşençay Basin. J. Geodyn. 37, 181–204.
Tsimi, C., Ganas, A., 2015. Using the ASTER global DEM to derive empirical relationships among facet slope, facet height, and slip rates along active normal faults. Geomorphology 234, 171–181.
Wallace, R.E., 1978. Geometry and rates of change of fault-generated range fronts, North-Central Nevada. J. Res. U.S. Geophys. Surv. 6, 637–650.
Wells, D.L., Coppersmith, K.J., 1994. New empirical relationships among magnitude, rupture length, rupture width, rupture area, and surface displacement. Bull. Seismol. Society Am. 84, 974–1002.